# Dynamics of dark-bright vector solitons in Bose-Einstein condensates

Majed O. D. Alotaibi and Lincoln D. Carr
*Department of Physics, Colorado School of Mines, Golden, Colorado 80401, USA*
(Received 3 July 2016; revised manuscript received 28 April 2017; published 5 July 2017)

We analyze the dynamics of two-component vector solitons, namely, dark-bright solitons, via the variational approximation in Bose-Einstein condensates. The system is described by a vector nonlinear Schrödinger equation appropriate to multicomponent Bose-Einstein condensates. The variational approximation is based on a hyperbolic tangent (hyperbolic secant) for the dark (bright) component, which leads to a system of coupled ordinary differential equations for the evolution of the ansatz parameters. We obtain the oscillation dynamics of two-component dark-bright solitons. Analytical calculations are performed for same-width components in the vector soliton, and numerical calculations extend the results to arbitrary widths. We calculate the binding energy of the system and find it to be proportional to the intercomponent coupling interaction and numerically demonstrate the breakup or unbinding of a dark-bright soliton. Our calculations explore observable eigenmodes, namely, the internal oscillation eigenmode and the Goldstone eigenmode. We find analytically that the number of atoms in the bright component is required to be less than the number of atoms displaced by the dark soliton in the other component in order to find the internal oscillation eigenmode of the vector soliton and support the existence of the dark-bright soliton. This outcome is confirmed by numerical results. Numerically, we find that the oscillation frequency is amplitude independent. For dark-bright solitons in $^{87}$Rb we find that the oscillation frequency range is 90 to 405 Hz and therefore observable in multicomponent Bose-Einstein condensate experiments.

DOI: 10.1103/PhysRevA.96.013601

## I. INTRODUCTION

Nonlinear waves have been a fascinating subject since the discovery of the solitary wave in 1834 by John Scott Russell in the Union Canal in Scotland, where he observed the "great wave of translation", as he called it at the time [1]. Since then, solitary waves of all kinds have been observed in many systems. Solitons in Bose-Einstein condensates (BECs), which are the subject of this article, have been the focus of research efforts since the creation of BECs [2,3].

A special structure of a coupled dark-bright soliton may exist in two-component BECs with repulsive interatomic interactions, where a dark soliton in one component creates a potential well that traps a bright soliton in the second component [4–10]. Although a bright soliton does not exist in a system with repulsive interactions [11], it can be supported in such a binary system due to the nonlinear interaction with the dark-soliton component. These solitons can be referred to as symbiotic [6,12]. A similar possibility for such a mechanism was proposed early in the literature in terms of a Bose-Fermi mixture in which bosons and fermions attract each other but the interaction between the bosons themselves is repulsive [13]. Vector solitons also exist in fiber optics [14–16], including bright-bright solitons [17] and dark-bright solitons [18]. Different types of vector solitons in multiple component BECs, such as pseudospinor BECs or three- and higher-component spinor BECs [19,20], can be created and transformed into each other by tuning the intercomponent interaction via Feshbach resonances [9,21,22]. Examples of these vector solitons in two-component BECs include bright-bright solitons [23,24] and dark-dark solitons [10,25], which exhibit rich dynamical far-from-equilibrium phenomena such as beating dark-dark solitons [26]. Among the techniques to create dark-bright solitons in a binary mixture of BECs are phase imprinting [4] and counterflowing of two binary BEC mixtures [27].

Many studies have been conducted to investigate the oscillation of vector solitons to gain better understanding of the dynamics of multicomponent nonlinear excitations. The oscillation of bright-bright solitons is one example of such studies. Another example is the oscillation of dark-dark solitons. In the case of dark-bright solitons, there have been investigations of the oscillation of multiple dark-bright solitons [6,27,28] and the oscillation of the internal modes for bright-bright solitons using a Gaussian ansatz [29] via variational approximation methods. However, to the best of our knowledge no one has treated the internal oscillations of the dark-bright-soliton case variationally using hyperbolic functions, which is the subject of this article. A popular choice for the ansatz in the variational approximation method is Gaussian functions for their relative ease in calculating integrals over the Lagrangian density. In addition, Gaussian functions do not impose any restriction on the choice of the width of the two components in the vector soliton. A disadvantage of using Gaussian functions is that they are less accurate than using hyperbolic functions; in fact, it is exactly the non-Gaussianity of solitons that sets them apart from wave-packet solutions to the linear Schrödinger equation. Thus in this article we perform calculations with variational approximation methods using the hyperbolic tangent (hyperbolic secant) for the dark (bright) component in the dark-bright soliton. This choice imposes restrictions on the width of the two components such that they must be identical in order to solve the integrals for the Lagrangian density analytically. We study the behavior of the dark-bright soliton when a phase is imprinted only on the bright component and find the oscillation modes of the system in addition to the binding energy and the velocity of the dark-bright soliton, which is affected by the interaction coefficient between the two components. In this scenario the moving bright component pulls the dark component along with it and oscillates in addition to moving the dark-bright soliton as a whole. One can think of this

 

mode as a vibrational excitation of the dark-bright "soliton molecule", as two-component vector solitons are sometimes called. We will use the term *dark-bright soliton* to describe these vector solitons. Our calculation shows that the system has a second oscillation mode in addition to the vibrational mode, namely, a Goldstone mode [30], as expected since the whole dark-bright soliton is moving.

This article is organized as follows. In Sec. II we study the oscillation of the two components in the dark-bright soliton by imprinting a phase on the bright component and finding the normal modes of the system by means of a variational approximation method based on a hyperbolic tangent (hyperbolic secant) for the dark (bright) soliton component for the two-component ansatz. In Sec. II D we calculate the binding energy between the bright and dark components in the dark-bright soliton as a function of the distance between the center of each component. In Sec. III we investigate dark-bright-soliton dynamics by numerically integrating the dimensionless nonlinear Schrödinger equation (NLSE) using an algorithm that is pseudospectral in time and adaptive Runge-Kutta in space. We focus on the intercomponent dynamics for different interaction coefficients and discuss real experimental values for the internal oscillation frequency in $^{87}$Rb. Finally, we present our conclusions in Sec. IV.

## II. ANALYTICAL CALCULATIONS

### A. Lagrangian density and ansatz

The two-component dark-bright soliton is governed by coupled NLSEs [2], which describe the evolution of the macroscopic wave functions of Bose condensed atoms:

$$\begin{aligned} i\hbar\frac{\partial}{\partial\tilde{t}}\tilde{u}(\tilde{x},\tilde{t}) &= -\frac{\hbar^2}{2m}\frac{\partial^2\tilde{u}(\tilde{x},\tilde{t})}{\partial\tilde{x}^2} \\ &\quad + [\tilde{g}_{11}|\tilde{u}(\tilde{x},\tilde{t})|^2 - \tilde{u}_0^2 + \tilde{g}_{12}|\tilde{v}(\tilde{x},\tilde{t})|^2]\tilde{u}(\tilde{x},\tilde{t}), \\ i\hbar\frac{\partial}{\partial\tilde{t}}\tilde{v}(\tilde{x},\tilde{t}) &= -\frac{\hbar^2}{2m}\frac{\partial^2\tilde{v}(\tilde{x},\tilde{t})}{\partial\tilde{x}^2} \\ &\quad + [\tilde{g}_{22}|\tilde{v}(\tilde{x},\tilde{t})|^2 + \tilde{g}_{21}|\tilde{u}(\tilde{x},\tilde{t})|^2]\tilde{v}(\tilde{x},\tilde{t}), \end{aligned} \tag{1}$$

where tildes denote dimensional quantities. The wave function of the dark soliton is given by $\tilde{u}(\tilde{x},\tilde{t})$, and that of the bright soliton is given by $\tilde{v}(\tilde{x},\tilde{t})$. The interaction strength, $\tilde{g}_{ij} = 2a_{ij}N\hbar\omega_\perp$ for $i,j = 1,2$ is renormalized to one dimension [31], where $\tilde{g}_{12}$ and $\tilde{g}_{21}$ are the interatomic interaction between the two components of the BEC and $\tilde{g}_{11}$ ($\tilde{g}_{22}$) represents the intra-atomic interaction for the dark (bright) component. The dark-soliton wave function is rescaled to remove the background contribution $\tilde{u}_0$, which is standard to avoid divergent normalization and energy [32]. The $s$-wave scattering length between components $i$ and $j$ is $a_{ij}$, $N$ is the total number of atoms, and $\omega_\perp$ is the oscillation frequency of the transverse trap. We assume the atomic masses for the two components $m_1$ and $m_2$ are equal to $m$, which is appropriate for the case of multiple hyperfine components of, e.g., $^{87}$Rb. To nondimensionlize Eqs. (1) we multiply them by $(\hbar\omega_\perp)^{-1}$ and scale all quantities according to the following units:

$$\begin{aligned} x &= \frac{\tilde{x}}{\ell_\perp}, \\ t &= \tilde{t}\omega_\perp, \\ g_{ij} &= \frac{\tilde{g}_{ij}}{\ell_\perp\hbar\omega_\perp}, \\ |u|^2 &= \ell_\perp|\tilde{u}|^2, \\ |v|^2 &= \ell_\perp|\tilde{v}|^2, \\ u_0^2 &= \frac{\tilde{u}_0^2}{\hbar\omega_\perp}, \end{aligned} \tag{2}$$

where $\ell_\perp = \sqrt{\hbar/(m\omega_\perp)}$ is the transverse harmonic oscillator length. In Sec. III D we discuss specific choices that are consistent with experimental observations. For simplicity we take $g_{11} \equiv g_1, g_{22} \equiv g_2$, and $g_{12} = g_{21} \equiv g$. The dimensionless NLSE becomes

$$\begin{aligned} i\frac{\partial u}{\partial t} &= -\frac{1}{2}\frac{\partial^2 u}{\partial x^2} + \left[g_1|u|^2 - u_0^2 + g|v|^2\right]u, \\ i\frac{\partial v}{\partial t} &= -\frac{1}{2}\frac{\partial^2 v}{\partial x^2} + [g_2|v|^2 + g|u|^2]v. \end{aligned} \tag{3}$$

We work with the dimensionless one-dimensional two-component coupled NLSE, Eq. (3), throughout the rest of this article. We use the normalization conditions

$$\int_{-\infty}^{\infty} dx\,\left(\frac{u_0^2}{g_1} - |u|^2\right) = \frac{N_1}{N}, \tag{4a}$$

$$\int_{-\infty}^{\infty} dx\,|v|^2 = \frac{N_2}{N} \tag{4b}$$

for the dark and bright components, respectively. Noting the background subtraction in the first component of Eqs. (4), $N_1$ is the number of atoms displaced by the dark soliton, in other words, the number of atoms involved in creating the density notch or minimum. Thus we define the total number of atoms $N$ involved in the dark and bright solitons as

$$N_1 + N_2 = N, \tag{5}$$

which is appropriate for the two-component BEC and standard for the dark-bright-soliton problem, thereby incorporating $N$ into the definition of the nonlinear coefficient $\tilde{g}_{ij}$ [2]. To obtain Eq. (3), we introduce the following Lagrangian density where we use Euler-Lagrangian equations to get the equations of motion, i.e., the coupled NLSE of Eq. (3):

$$\begin{aligned} \mathcal{L} &= \frac{i}{2}\left[u^*\frac{\partial u}{\partial t} - u\frac{\partial u^*}{\partial t}\right]\left[1 - \frac{u_0^2}{g_1|u|^2}\right] - \frac{1}{2}\left|\frac{\partial u}{\partial x}\right|^2 \\ &\quad - \frac{1}{2}\left[\sqrt{g_1}|u|^2 - \frac{u_0^2}{\sqrt{g_1}}\right]^2 + \frac{i}{2}\left[v^*\frac{\partial v}{\partial t} - v\frac{\partial v^*}{\partial t}\right] \\ &\quad - \frac{1}{2}\left|\frac{\partial v}{\partial x}\right|^2 - \frac{g_2}{2}|v|^4 - g|u|^2|v|^2 \\ &\quad + \frac{u_0^2}{2g_1}[2\theta_2(x + d(t)) + \theta_1(t)]^2. \end{aligned} \tag{6}$$

Note that the last term does not depend on the wave function of the dark or the bright component and was added to eliminate the infinity when using the ansatz, Eq. (7), with $\theta_1$ and $\theta_2$ to be defined in the following. We adopt the following trial functions as the dark-bright-soliton solutions to Eq. (3):

$$\begin{aligned} u(x,t) &= \frac{u_0}{\sqrt{g_1}}\left\{iA + c\tanh\left[\frac{(d(t)+x)}{w}\right]\right\} \\ &\quad\times \exp(i\{\theta_0 + [d(t)+x]\theta_1(t) + [d(t)+x]^2\theta_2\}), \\ v(x,t) &= \frac{u_0}{\sqrt{g_2}}F\ \mathrm{sech}\left[\frac{(b(t)+x)}{w}\right] \\ &\quad\times \exp(i\{\phi_0 + [b(t)+x]\phi_1(t) + [b(t)+x]^2\phi_2\}). \end{aligned} \tag{7}$$

The parameters $A$, $c$, and $F$ describe the amplitude of the two components, where $A^2 + c^2 = 1$, which is standard in the formulation of an NLSE dark soliton [33]. In the exponential terms, $\phi_0$ and $\theta_0$ give rise to a complex amplitude. $\phi_1(t)$ and $\theta_1(t)$ are responsible for the dark- and bright-component velocities. Note that the velocity of a dark soliton also depends on the amplitude of the wave function as shown in Eq. (9d); $\phi_2$ and $\theta_2$ are essential to vary the width [34], and $d(t)$ and $b(t)$ are the positions of the dark and bright solitons, respectively. The two components are assumed to have the same width $w$. To study the oscillation of the two components in time, we chose the variational parameters to be the two component positions $d(t)$ and $b(t)$ and the phases $\theta_1(t)$ and $\phi_1(t)$. As mentioned in Sec. I, the analytical calculations use hyperbolic functions as an ansatz, which is more accurate than using Gaussian functions. This choice requires the two components have identical width in order for the problem to remain analytically tractable, as opposed to using a Gaussian ansatz [29]. However, we will relax this constraint in Sec. III. Using the ansatz [Eqs. (7)] in the normalization [Eqs. (4)], we find the relation between $N_1, N_2$, and the coefficients of the two components in the dark-bright soliton:

$$\frac{2c^2u_0^2w}{g_1} = \frac{N_1}{N}, \quad \frac{2F^2u_0^2w}{g_2} = \frac{N_2}{N}. \tag{8}$$

### B. Evolution equations

Substituting Eq. (7) into the Lagrangian density equation (6) and integrating over space from $-\infty$ to $\infty$ results in the Lagrangian as a function of the variational parameters. Applying the Euler-Lagrange equations then yields a system of ordinary differential equations (ODEs) that describes the evolution in time of the position and phase for both components:

$$\begin{aligned} \frac{d}{dt}\phi_1(t) &= \alpha\ \mathrm{csch}\left(\frac{b(t)-d(t)}{w}\right)^4 \\ &\quad\times\left\{2[b(t)-d(t)]\left[2+\cosh\left(2\frac{b(t)-d(t)}{w}\right)\right]\right. \\ &\quad\left.-3w\sinh\left(2\frac{b(t)-d(t)}{w}\right)\right\}, \end{aligned} \tag{9a}$$

$$\frac{d}{dt}\theta_1(t) = \beta\frac{d}{dt}\phi_1(t), \tag{9b}$$

$$\frac{d}{dt}b(t) = -\phi_1(t), \tag{9c}$$

$$\frac{d}{dt}d(t) = -\gamma - \theta_1(t), \tag{9d}$$

where

$$\alpha \equiv \frac{c^2gu_0^2}{g_1w^2}, \quad \beta \equiv \frac{F^2g_1}{c^2g_2}, \quad \gamma \equiv \frac{A}{cw}. \tag{10}$$

Equations (9) can be reduced to one second-order ODE:

$$\begin{aligned} \frac{d^2}{dt^2}l(t) &= (\beta-1)\alpha\ \mathrm{csch}\left(\frac{l(t)}{w}\right)^4 \\ &\quad\times\left\{2l(t)\left[2+\cosh\left(\frac{2l(t)}{w}\right)\right]-3w\sinh\left(\frac{2l(t)}{w}\right)\right\}, \end{aligned} \tag{11}$$

where $l(t) \equiv b(t) - d(t)$. Despite the attractive simplicity of this unified description, it is physically advantageous to address the problem with Eqs. (9) to illustrate the behavior of the evolution of the variational parameters in time and to clarify the physical meaning of the fixed point and linear stability analysis in the next section.

### C. Normal modes

Equations (9) possess one stable fixed point:

$$\phi_1 = 0, \quad \theta_1 = -\gamma, \quad l = 0. \tag{12}$$

Since $l = 0$, we can choose the original of the coordinate system such that $b = d = 0$. In the Appendix we prove that Eqs. (9) with the fixed point $l = 0$ do not possess a singularity. We proceed by linearizing Eqs. (9) around the fixed point equation (12), i.e., $a_i(t) = a_{\mathrm{fp}} + \delta a e^{i\omega t}$, where $a_i$ represents the variational parameters and $a_{\mathrm{fp}}$ is the fixed point mentioned above. This results in a matrix equation of the form

$$\begin{bmatrix} i\omega & 0 & -A_1 & A_1 \\ 0 & i\omega & -A_2 & A_2 \\ 1 & 0 & i\omega & 0 \\ 0 & 1 & 0 & i\omega \end{bmatrix}\begin{bmatrix} \delta\phi_1 \\ \delta\theta 1 \\ \delta b \\ \delta d \end{bmatrix} = \begin{bmatrix} 0 \\ 0 \\ 0 \\ 0 \end{bmatrix}, \tag{13}$$

where

$$A_1 = \left(8c^2gu_0^2\right)/(15g_1w^2), \tag{14}$$

$$A_2 = \left(8F^2gu_0^2\right)/(15g_2w^2). \tag{15}$$

Taking the determinant of the matrix and solving for eigenfrequencies $\omega$ and the associated eigenvectors yields

$$v_{\mp} = \begin{bmatrix} \mp\frac{2}{\sqrt{15}}(N_1/N_2)w^{-\frac{3}{2}}\sqrt{g}\sqrt{\frac{N_2-N1}{N}} \\ \mp\frac{2}{\sqrt{15}}w^{-\frac{3}{2}}\sqrt{g}\sqrt{\frac{N_2-N1}{N}} \\ N_1/N_2 \\ 1 \end{bmatrix}, \tag{16a}$$

$$v_{01} = \begin{bmatrix} 0 \\ 0 \\ 1 \\ 1 \end{bmatrix}, \quad v_{00} = \begin{bmatrix} 0 \\ 0 \\ 0 \\ 0 \end{bmatrix}, \tag{16b}$$

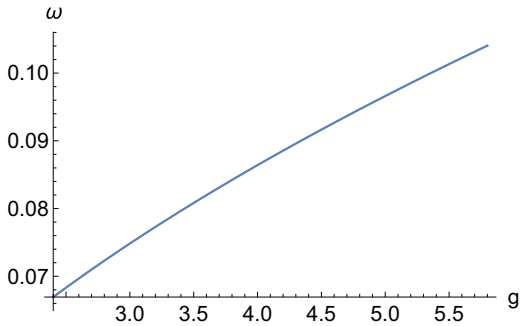


FIG. 1. Oscillation frequency of the two components in the dark-bright soliton versus the interaction coefficients $g$. We set $N_1 \approx 0.503 \times 10^5$ atoms and width $w = 1$, where $\omega$ and $g$ are unitless. The range of the values in $g$ is from 2.4 to 5.8, matching the range of $g$ in the numerical calculations.

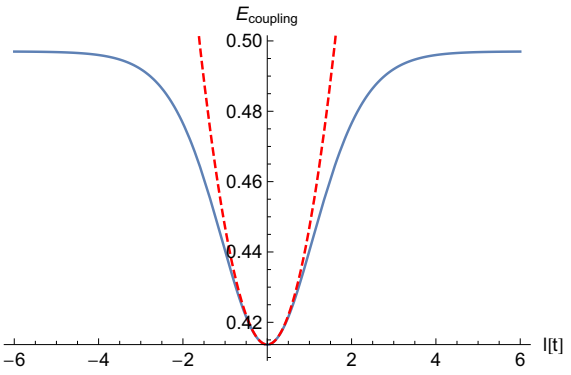


FIG. 2. Coupling energy versus the distance between the two components $l(t)$ when $t = 0$. Here we normalize the interaction coefficients to unity and set $N_1 \approx 0.503 \times 10^5$ atoms. The solid blue line represents Eq. (19), and the dashed red line represents Eq. (20).

and eigenfrequencies [35]

$$\omega_{\mp} = \mp 2i\sqrt{\frac{1}{15}}\sqrt{g}w^{-\frac{3}{2}}\sqrt{(N_2 - N_1)/N}, \tag{17a}$$

$$\omega_{01} = 0,\ \omega_{00} = 0, \tag{17b}$$

where the oscillation frequency $\omega_{01}$ in Eq. (17b) corresponds to the zero-energy mode, sometimes defined in the literature as a Goldstone mode [30,36], and we have used the normalization equations (4). This mode breaks translational symmetry with no energy cost. We can interpret it as a moving dark-bright soliton without internal oscillation of the two components. Also, the eigenvector of this mode $\nu_{01}$ shows no contribution from the phases that are responsible in the first place for the oscillation and has $b$ and $d$ moving together with zero frequency, i.e., at constant velocity.

Turning to the nonzero frequency eigenmode, in Eq. (17a), stable oscillation requires the condition $N_1 > N_2$ be met, in other words, $g_2 > \frac{F^2}{c^2} g_1$. Thus for the same amplitude components there is no oscillation. This result is supported by the numerical calculations in Sec. III A, where we find that the bright component in the dark-bright soliton does not exist when the total number of atoms in the bright component is equal to or greater than the total number of atoms displaced by the dark soliton in the other component (see Fig. 3 below). Using $N_2 = N - N_1$, we can rewrite the oscillation frequency as

$$\omega_{\mp} = \mp 2\sqrt{\frac{1}{15}}w^{-\frac{3}{2}}\sqrt{g}\sqrt{(2N_1/N) - 1}. \tag{18}$$

Note that for a real oscillation the normalization constant $2N_1/N$ should be greater than 1, which in turn makes $N_1 > N_2$. Considering the typical number of atoms in the $^{87}$Rb experiment, we set $N = 10^5$ and $N_1 \approx 0.503 \times 10^5$. Setting $w = 1$ in Eq. (18), we plot the relative frequency versus the interaction coefficient $g$ in Fig. 1.

### D. Binding energy of the vector soliton

In the Lagrangian density, Eq. (6), the term $g|u|^2|v|^2$ represents the coupling interaction per unit space between the two components of the dark-bright soliton. Using the ansatz (7), we can integrate this term over $x$ to find the coupling interaction of the system. The binding energy can be found when we subtract the coupling interaction energy at $l = 0$ from $l = \infty$, where $l$ is the separation between the bright and dark solitons. The energies associated with all other terms in the Lagrangian density turn out to be independent of $l$. The coupling interaction energy of the system is

$$E_{\text{coupling}} = \frac{F^2 g u_0^4}{g_1 g_2}\text{csch}\left[\frac{l(t)}{w}\right]^2 \times \left\{4c^2\left(w - l\coth\left[\frac{l(t)}{w}\right]\right) + 2w\sinh\left[\frac{l(t)}{w}\right]^2\right\}. \tag{19}$$

In Fig. 2 we plot Eq. (19). As expected for a binding energy, the coupling interaction energy is minimum at the center, where the locations of the bright-soliton maximum and dark-soliton minimum coincide. Applying a phase to the bright component, i.e., giving it a "kick", causes it to experience a force due to the coupling interaction energy that brings it back to the energy minimum, which creates an oscillation between the two components. If the imprinted phase is large enough to separate the two solitons beyond their relative widths, the system reaches a point where the bright soliton escapes and is then destroyed, as we will show in Sec. III.

To analytically explore the behavior of the oscillation around the fixed point when $l \ll 1$ we expand Eq. (19) to quadratic order in $l$:

$$E_{\text{coupling}} = \frac{2(3 - 2c^2)F^2 g u_0^4 w}{3g_1 g_2} + \frac{8c^2 F^2 g u_0^4}{15 g_1 g_2 w} l^2. \tag{20}$$

As a result, we see that the coupling energy when $l \ll 1$ behaves as a parabolic potential energy near the fixed point. Therefore we should expect the oscillation frequency to be amplitude independent for small amplitude excitations, and this is indeed the result we obtain in Sec. III (see Fig. 7).

We can treat the coupling energy as a potential energy and derive the equation of motion for $l(t)$:

$$m\frac{d^2}{dt^2}l(t) = -\frac{d}{dl}E_{\text{coupling}} = \frac{2c^2F^2gu_0^4}{g_1g_2w} \times \operatorname{csch}\left(\frac{l(t)}{w}\right)^4\left\{2l(t)\left[2+\cosh\left(\frac{2l(t)}{w}\right)\right] - 3w\sinh\left(\frac{2l(t)}{w}\right)\right\}, \quad (21)$$

where $m = 1$ in our units. Comparing Eq. (21) to Eq. (11), we find that the two equations are different only by the coefficients and therefore yield different frequencies. This can be understood by examining the Lagrangian density, Eq. (6), where we subtract the background contributions from the dark-soliton momentum term and the intracomponent mean-field energy term. The calculations leading to Eq. (11) account for this subtraction, whereas the calculations leading to Eq. (21) do not. Consequently, the coefficients are different.

By taking the difference between Eq. (19) at $l = 0$ and $l = \infty$ we find the binding energy:

$$E_{\text{binding}} = E_{\text{coupling}(l\to 0)} - E_{\text{coupling}(l\to\infty)} = -\frac{4c^2F^2gu_0^4w}{3g_1g_2}. \quad (22)$$

We note that the binding energy is thus proportional to the intercomponent coupling $g$ and inversely proportional to the intracomponent couplings $g_1$, $g_2$. The latter inverse proportionality is due to normalization. In addition, we calculate the kinetic energy $E_{\text{K}}$ and the intracomponent mean-field energy $E_{\text{MF}}$ of the dark and bright components separately and compare them to the binding energy above.

For the dark component in the dark-bright soliton,

$$E_{\text{K}} = \frac{N_1\left[-2+\pi^2w^4\theta_2^2\right]}{6Nw^2} + \frac{1}{2}\theta_1\left(\frac{4Acu_0^2}{g_1} + \frac{N_1\theta_1}{N}\right), \quad (23)$$

$$E_{\text{MF}} = -\frac{g_1N_1^2}{6wN^2}. \quad (24)$$

For the bright component in the dark-bright soliton,

$$E_{\text{K}} = -\frac{N_2\left[1+\pi^2w^4\phi_2^2\right]}{6Nw^2} - \frac{N_2\phi_1^2}{2N}, \quad (25)$$

$$E_{\text{MF}} = -\frac{g_2N_2^2}{6wN^2}. \quad (26)$$

We found $E_{\text{K}}$ and $E_{\text{MF}}$ of the dark- (bright-) soliton component are inversely proportional to the intracomponent coupling $g_1$ ($g_2$). Note that neither $E_{\text{K}}$ nor $E_{\text{MF}}$ of the two components depends on the intercomponent coupling $g$ as expected. This result can be understood when we examine the Lagrangian density, Eq. (6), where the intercomponent coupling $g$ appears only in the coupling term and therefore contributes only to the binding energy.

Finally, we compare the binding energy to the kinetic energies [i.e., Eqs. (23) and (25)] and the mean-field energies [i.e., Eqs. (24) and (26)] of the dark-bright soliton. We find that in order to break or unbind the dark-bright soliton the imprinted phase on the bright component should be greater than the following quantity:

$$\phi_1 > \frac{1}{\sqrt{3N_2}}\left[-\frac{2N_1+N_2-2N_1w}{w^2} - \frac{N_1^2(2+g_1)+g_2N_2^2}{Nw} + \pi^2w^2\left(N_1\theta_2^2-N_2\phi_2^2\right)+3N_1\theta_1^2 + \frac{6\theta_1\sqrt{N_1}\sqrt{2Nu_0^2w-g_1N_1}}{w\sqrt{g_1}}\right]^{-1}. \quad (27)$$

In Sec. III B, we compare Eq. (27) to Fig. 9.

## III. NUMERICAL CALCULATIONS

In this section we numerically investigate the interaction between the two components. First, we explore the approach to the integrable Manakov case of equal interaction coefficients $g = g_1 = g_2$ and find the ground-state density of a dark-bright soliton. The Manakov case formally precludes a dark-bright soliton since the number of atoms in the bright-soliton component must be less than the number of atoms displaced by the dark-soliton component. In Sec. II C we derived this condition as a requirement to find the real oscillation of the two-component dark-bright soliton. Second, we investigate the interaction between the two components with unequal interaction coefficients by finding the ground state of the system when the interatomic interaction goes from the miscible to the immiscible domain, representing a quantum phase transition for the dark-bright soliton. Third, we investigate dark-bright-soliton dynamics, studying the velocity of the dark-bright soliton, the oscillation frequency mode as a function of the interaction coefficients, and the unbinding or breakup process when the dark-bright soliton is too strongly perturbed. Fourth, we end this section with a discussion of the experimental case for $^{87}$Rb where we can use these units to convert between the dimensionless variables in the study conducted and physically measurable quantities such as the oscillation time. Note that throughout this section, we performed the simulations with grid size $n_x = 256$ in a box with hard-wall boundaries. The box length was set to $L = 50$ unless otherwise noted.

### A. Dark-bright soliton with equal interaction coefficients

We obtain our initial state numerically by using the imaginary-time-propagation method to find the ground-state energy of the coupled NLSEs. Starting with constant initial wave functions for both components, where we imprinted a phase on only the constant dark component, we perform two sets of simulations. We allow the particle number to fluctuate between the two components during imaginary-time propagation. Fixing $g_1 = g_2 = 1$ and allowing $g$ to increase toward the Manakov case of $g = g_1 = g_2$, we find the result shown in Fig. 3, where in the last two panels the dark-bright soliton ceases to exist and all atoms pile up in the "bright" component.

### B. Dark-bright soliton with unequal interaction coefficients

We explore the miscible-immiscible quantum phase transition at $g^2 = g_1g_2$ in a non-Manakov system for which $g_1 \neq g_2$,

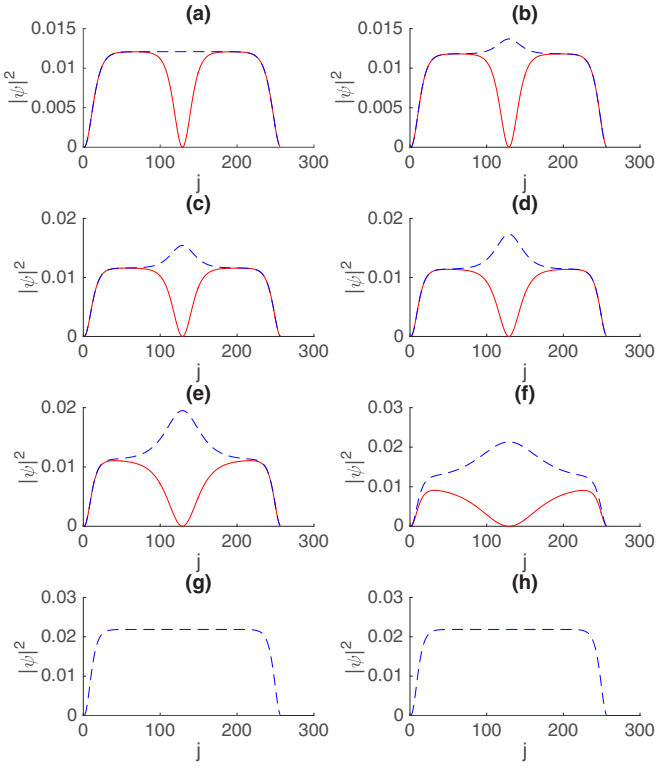


FIG. 3. Approach to the Manakov case. Ground-state density of a two-component BEC when the interaction coefficients $g_1, g_2$ are equal to unity versus the coupling interaction coefficient $g$. The bright (dark) component is the dashed blue (solid red) line. In (a)–(h) $g =$ 0.0,0.2,0.4,0.6,0.8,0.95,1.0,1.2, respectively. We allow the relative particle number between the two components to fluctuate, and past the Manakov point at $g = 1$ the lowest-energy solution places all atoms in one component.

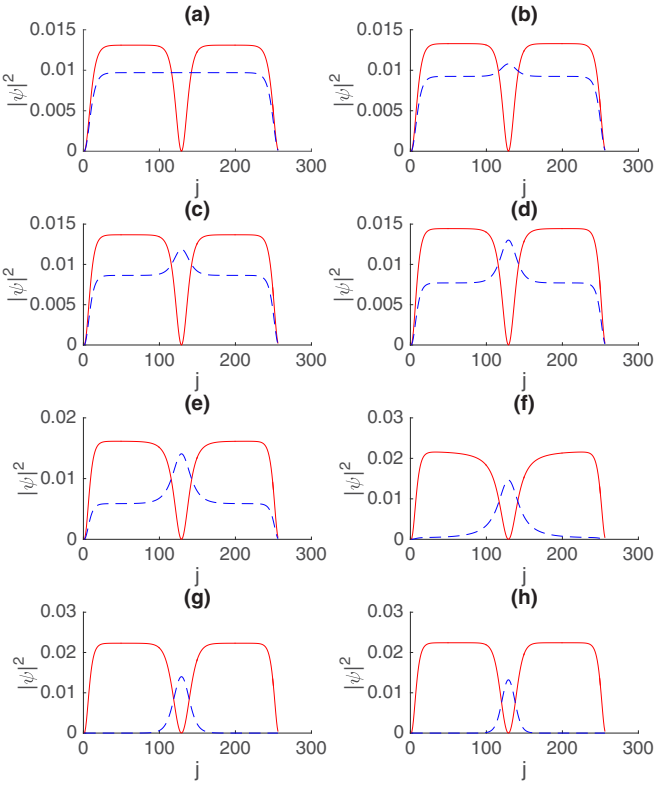


FIG. 4. Dark-bright solitons through the miscible-immiscible phase transition. We take $g_1 = 2.0$ and $g_2 = 2.7$. In (a)–(h) $g =$ 0.0,0.4,0.8,1.2,1.6,2.0,2.4,2.8, respectively. The phase transition occurs at $g = 2.3$, leading to well-localized bright solitons in the immiscible domain in the last two panels.

as shown in Fig. 4, where we again tune $g$ through the transition. For $g < 2.3$ we do not find a true bright soliton but rather a bump on a nonzero background, in fact, a finite-size effect. For $g > 2.3$ in the last two panels the dark-bright soliton appears since the number of atoms in the bright component is less than that displaced by the dark component. In the miscible domain in Figs. 4(a)–4(f), the strength of the repulsive interaction between the two components is less than the repulsive interaction between the particles in the bright component, which allows the bright soliton to expand and reach the boundaries. In the immiscible domain in Figs. 4(g) and 4(h), the coupling interaction is strong to the point that it forces the bright component to live within only the dark soliton.

To highlight the effect of the miscibility transition, in Fig. 5, as we increase the intercomponent coupling $g$, the amplitude of the bright component decreases, and the amplitude of the dark component increases. With increasing intercomponent coupling $g$, the ground state of the dark-bright soliton shows that the density of the bright component decreases, and therefore the amplitude does too. This can be understood by examining Fig. 4. We see that when the intercomponent coupling is zero, the sizes of the two densities of the dark and bright components are governed by intracomponent couplings $g_1$ and $g_2$, respectively. As we increase $g$, the dark-component density exerts a repulsive force on the bright-component density and forces it to localize in the center. As we pass the phase-transition point when $g > 2.3$, the density of the bright-soliton component continues to decrease; thus its amplitude decreases too, and the density of the dark-soliton component increases at a slow rate compared to the change in the bright-component density. The difference between the rate of change with $g$ in the density between the two components depends on their sizes. The dark-soliton component is larger than the bright-soliton component, as shown in Fig. 4, and therefore increasing the density of the dark-soliton component will have a small effect on increasing its amplitude. Finite-size effects allow the soliton to exist slightly beyond the miscibility boundary indicated by the dashed line in Fig. 4.

### C. Dark-bright-soliton dynamics

We now turn to internal excitations of the dark-bright soliton. Our procedure is to imprint a phase solely on the bright component via state-selective manipulation of BECs. The ensuing dynamics involves not only internal oscillations but also an overall velocity of both dark and bright components, i.e., the Goldstone mode. The results for our two case studies from Fig. 5 are shown in Fig. 6. We find the velocity of the dark-bright soliton drops quickly at the beginning; then it slowly decreases as the coupling interaction increases. This behavior can be understood if we examine the density of

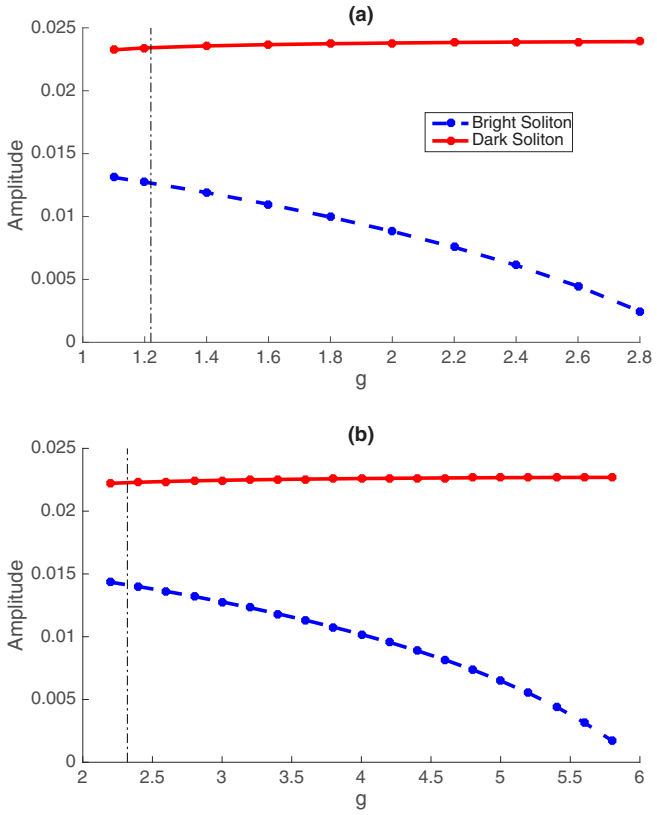


FIG. 5. Amplitude of the bright and dark components versus the coupling interaction $g$. We measure the amplitudes of the two components at the ground state with different values of $g_1$, $g_2$, and $g$. (a) $g_1 = 1.0, g_2 = 1.5$ and (b) $g_1 = 2.0, g_2 = 2.7$.

the bright component. We find the form depicted in Fig. 5; that is, the amplitude (and therefore the density) of the bright component decreases as the coupling interaction increases. In this case, the imprinted phase on the "small" bright component will not pull the dark soliton quickly, and therefore the velocity of the dark-bright soliton changes at a small rate as the bright-component amplitude decreases. In addition, the initial velocity of the dark-bright soliton when $g_1 = 2.0$ and $g_2 = 2.7$ is higher than the case when $g_1 = 1.0$ and $g_2 = 1.5$ because the difference between the amplitudes of the two components in the former case is less than in the latter. In other words, a phase imprinted on the bright component will have a bigger impact in the former case. The dashed lines distinguish the miscible and immiscible domains. Note that a dark-bright soliton can be created as we approach this line from the miscible domain.

Having explicated the trends in the overall velocity or Goldstone mode, we examine our second mode of interest, namely, the frequency of internal excitations. In Fig. 7, we first discuss the numerical results; then we will discuss the comparison between these outcomes and the analytical results. Numerically, different values of imprinted phases on the bright component are shown ($\phi = 0.7$ and $\phi = 1.0$). The oscillation frequencies of the two components versus the coupling interaction $g$ are almost identical, indicating that the frequency is amplitude independent. Imprinting a large phase on the bright component can decouple the two components in the dark-bright soliton. In the case with $\phi = 1.0$ the imprinted

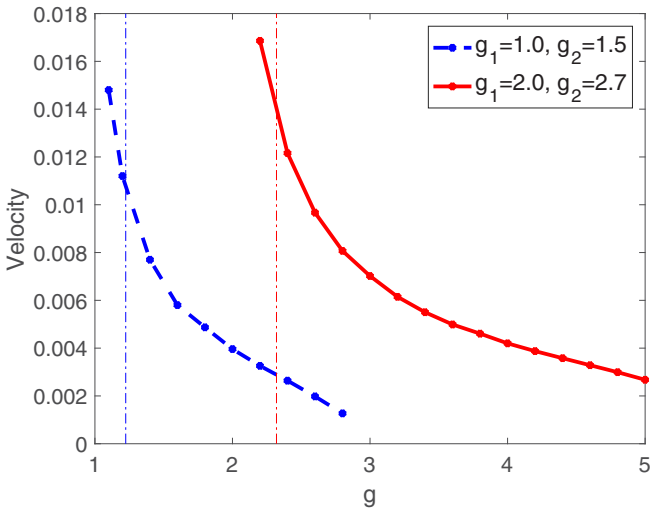


FIG. 6. Collective velocity of dark-bright soliton after phase imprint. We take a phase imprint of $\phi = 0.5$ and two different cases for $g_1$ and $g_2$ in the immiscible domain when $g > \sqrt{g_1 g_2}$. See Sec. III D for converted units. Note that a dark-bright soliton can be created as we get very close to this line from the miscible domain. The amplitude of the bright soliton controls the rate of the velocity of the dark-bright soliton. As we increase the intercomponent coupling interaction $g$, the amplitude of the bright soliton decreases as shown in Fig. 5, and therefore the density of the bright soliton decreases too. Imprinting a phase on the low-density bright soliton will have a small effect on dragging the dark soliton and therefore will result in a low velocity of the dark-bright soliton.

phase is large enough to cause a disturbance when the coupling coefficient is close to the miscible domain, and therefore it shows a different oscillation frequency for $g$ just above the critical value for the phase transition. In Fig. 7 we also plot the analytical results obtained from Eq. (18). We did not

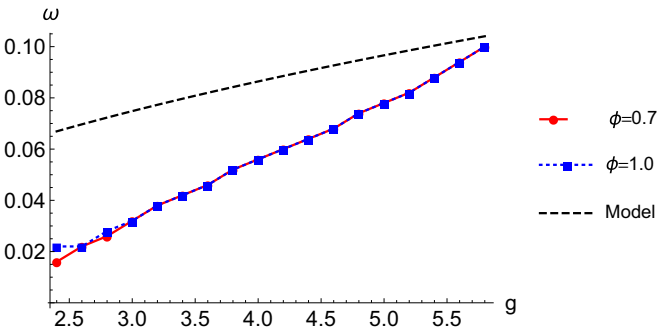


FIG. 7. Trends in internal dynamics. Oscillation frequency of the two components in the dark-bright soliton, with $g_1 = 2.0$, $g_2 = 2.7$, and $\phi = 0.7$ and 1.0, obtained from numerical integration of Eq. (3) versus the oscillation frequency obtained from the analytical calculations, Eq. (18). Numerically, the oscillation frequency of the two components versus the coupling coefficient $g$ for different values of $\phi$ shows that the oscillation frequency is amplitude independent in the case explored. We also plot the result from Eq. (18) to compare the two outcomes from the analytical and numerical calculations. The discrepancy between numerics and the model is due to the restricted ansatz (equal soliton widths) in the variational calculation.

include the oscillation of the width, i.e., the breather mode, in the analytical calculations because we can only perform the calculations for in-phase width oscillation analytically. In contrast, in the numerical calculations the motion also includes arbitrary-phase width oscillation. The range of the values of $g$ is bounded between two limits. In the lower limit, when $g < \sqrt{g_1 g_2}$, i.e., in the miscible domain, the bright component in the dark-bright soliton exists on top of a finite background caused by finite-size effects (for example, see Fig. 4). Therefore imprinting the phase on the bright-soliton component to start the oscillation motion will also move the finite background density, causing a larger-scale disturbance and affecting the frequency results. The upper limit of the values of $g$ come from the fact that for large $g$ the ground-state energy of the system does not support a dark-bright soliton because of the strong intercomponent interactions between the dark component and the bright component.

We see also in Fig. 7 that the comparison between the numerical and analytical results becomes better as we increase the intercomponent interactions $g$. When $g$ is close to the miscible domain, the oscillation of the width of the two components is stronger due to the fact that $g$ is small, and therefore the width oscillation contributes to the oscillation of the two components. When $g$ is large, the oscillation of the width of the two components becomes smaller due to the fact that the repulsive interaction between the two component is stronger, and therefore it will force the two components to be confined in their region. Thus as we increase $g$, we will have a smaller contribution of the width oscillation mode in the oscillation of the two components, which will improve the comparison between the numerical and analytical results.

To explain the data underlying Figs. 6 and 7, we show an example of the complete numerical integration and the resulting density and phase of the two-component wave function in Fig. 8. To obtain these data, we numerically integrate Eq. (3) using a pseudospectral method as mentioned in Sec. I. Figure 8 clarifies many features of the interactions between the two components in the dark-bright soliton. Figures 8(a) and 8(b) show the density and the phase of the oscillating bright component, while Figs. 8(c) and 8(d) show the corresponding dark-component oscillations. Figures 8(e)–8(h) present a close-up of a small interval to display the oscillation more clearly. The interaction coefficients are $g_1 = 2.0$, $g_2 = 2.7$, $g = 3.2$, and $\phi = 0.7$. The oscillation frequency amplitude of the dark component decreases as we increase the interaction coefficient, which in turn makes the observation of the oscillation in the dark component not obvious compared to the oscillation of the bright component. For the above interaction coefficient values the amplitude of the bright component is almost half the amplitude of the dark component, as shown in both Figs. 8 and 5.

Finally, we examine the breakup of a dark-bright soliton. In Fig. 9, we again plot the dark-bright-soliton density and phase in both components, but this time we imprint a relatively large phase on the bright-soliton component in order to unbind the dark-bright soliton. We emphasize that the bright component of a dark-bright soliton can exist only at long times in the bound form. When the imprinting phase is large (i.e., $\phi =$ 6 and 10), a significant portion of the bright-soliton density escapes from the effective potential created by the dark-soliton

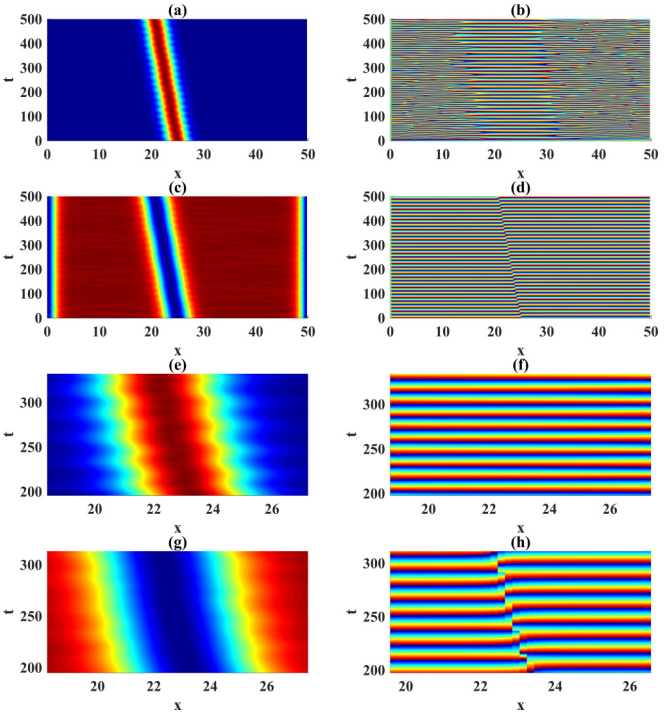


FIG. 8. Oscillation of the two-component wave function $|u(x,t)|^2$ and $|v(x,t)|^2$ in the immiscible domain with $g_1 = 2.0$, $g_2 = 2.7$, $g = 3.2$, and $\phi = 0.7$. (a), (b), (c), and (d) represent the density and the phase of the bright and dark components, respectively. In (e), (f), (g), and (h) we plot the preceding images with small time and space intervals to show the oscillations.

component (see Fig. 10) and therefore breaks up the dark-bright soliton. Using the interaction coefficients mentioned in Fig. 9 in Eq. (27) in addition to setting $N_1 \approx 0.503 \times 10^5$, $N = 1 \times 10^5$, $\theta_1 = 1$, $\phi_2 = 1$, $\theta_2 = 2$, and $w = 1$, we find that the system oscillates as long as $\phi < 3.4$. Above this value the dark-bright soliton starts to unbind or break up. We find this value to be in good agreement with the numerical results obtained in Fig. 9, where we see that a significant fraction of the bright-soliton component breaks away from the effective potential created by the dark-soliton component around $\phi = 6$ and greater.

To quantify the breakup, in Fig. 10 we plot the percentage of density loss of the bright component in the dark-bright soliton as a function of time for different phase-imprinting values. Below the critical value of $\phi$, the bright-component density is almost intact. Above the critical value the bright component starts to lose a significant portion of the density, characteristic of the breaking up of the dark-bright soliton. The integration region for the bright-component density is taken to be the line extending a distance $r$ on either side of the dark-component center $r_0$. Therefore the local bright-component density is given by

$$E_{BS} = \int_{r_0-r}^{r_0+r} dx\ |v|^2. \tag{28}$$

We interpret the dark-soliton-component center as the point of minimum density. We define numerically the distance $r = c_1(L/n_x)$, where $L$ and $n_x$ represent box dimension and grid

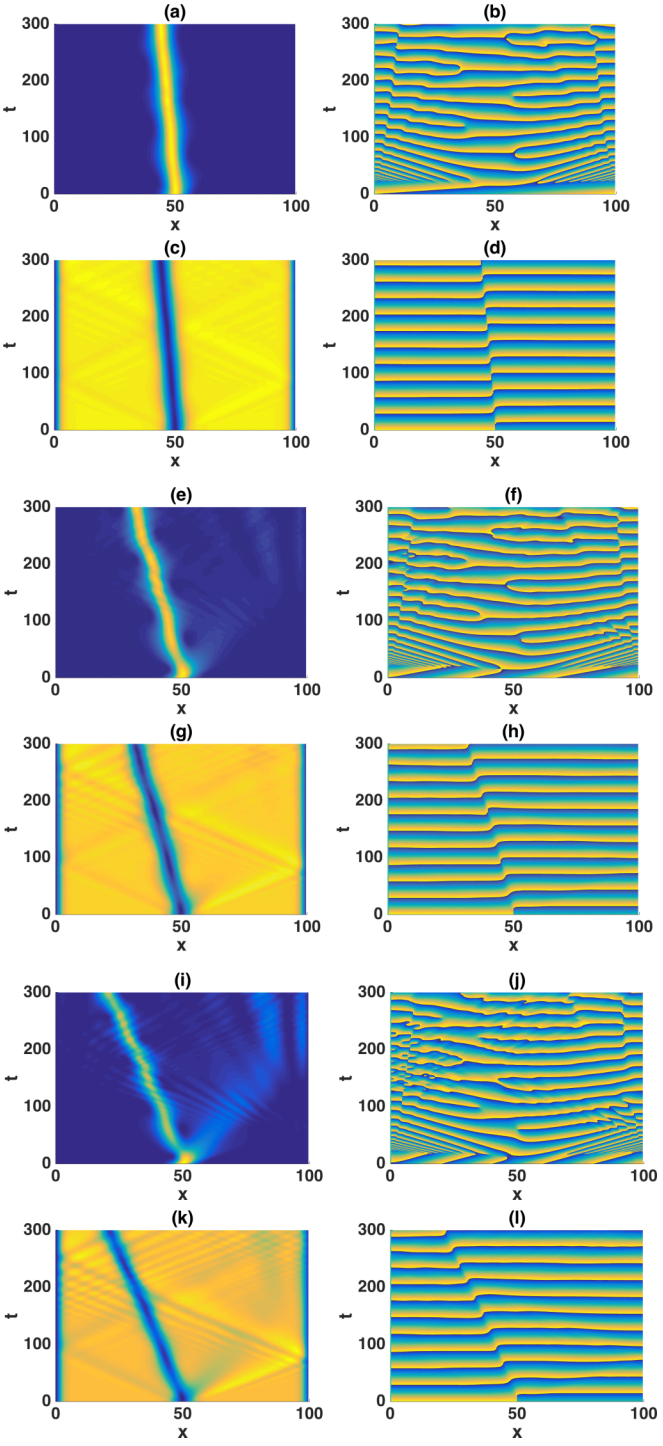


FIG. 9. Unbinding of a dark-bright soliton. We demonstrate the breakup of the dark-bright soliton by imprinting different values of the phase $\phi$ on the bright component with interaction coefficients $g_1 = 2.0$, $g_2 = 2.7$, $g = 2.6$. (a)–(d), (e)–(h), and (i)–(l) use phase imprintings of $\phi = 2$, 6, and 10, respectively. The left (right) panels show the density (phase) of the bright and dark components. The box dimension is $L = 100$.

size, respectively. The factor $c_1 = 50$ defines the cutoff region, which is wide enough to capture the dark-component area, as can be seen in Fig. 9.

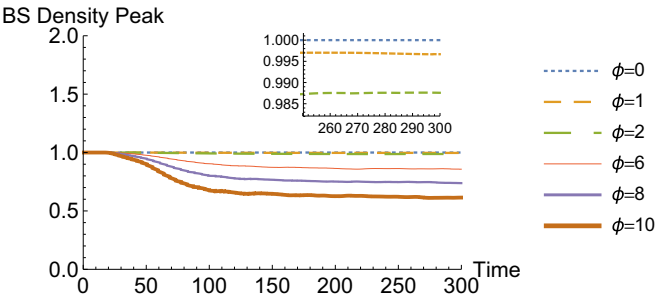


FIG. 10. Percentage density loss of the bright component in the dark-bright soliton for different phase-imprinting values. Below the critical value mentioned above (i.e., $\phi = 0$, 1, and 2) the dark-bright soliton maintains its internal structure, and the bright-soliton component density is almost intact; see the inset. Above the critical value (i.e., $\phi = 6, 8$, and 10) we see that the bright soliton loses density due to the relatively strong kick that allows for a significant portion of the density to escape. The inset also highlights the stability of the dark-bright soliton at long times for small enough phase imprinting.

### D. Units

Typical experimental values for a $^{87}$Rb BEC are $\omega_\perp \approx 2\pi \times 720$ Hz, $a_s \approx 5.1 \times 10^{-9}$m, and $N \approx 10^5$. For these parameters, the length scale is $\ell_\perp \approx 0.4$ $\mu$m, and the time scale is $t_\perp \approx 0.22$ ms.

An example of using the units in Table I to calculate the frequency of the oscillation mode in $^{87}$Rb is obtained by examining Fig. 7. For $g = 4$ we find that the oscillation frequency $\omega$ is 0.056. Using the units in Table I, the equivalent SI units are $\omega = 252$ Hz with $g = 54.8\ k_B$ nK $\mu$m, which are reasonable numbers for an experiment in $^{87}$Rb.

## IV. CONCLUSIONS

We calculated the normal modes of the system using the hyperbolic tangent for the dark component and the hyperbolic secant for the bright component. We found the velocity of each component depends on the imprinted phase, following the known expression for the velocity of the condensate in which the phase depends on $x$ in order to cause the dark-bright-soliton components to move. In the dark component, the velocity also depends on the amplitude. There are two modes of the oscillation of the dark-bright soliton, the Goldstone mode, which we interpreted as a moving dark-bright soliton without internal oscillation of the two components, and the oscillation mode of the two components relative to each other. In addition,

TABLE I. Converted units.

| SI units | Factor per unit | Unitless | Unit |
|---|---|---|---|
| $\tilde{x}$ | $0.4 \times 10^{-6}$ | $x$ | meters |
| $\tilde{t}$ | $0.22 \times 10^{-3}$ | $t$ | seconds |
| $\tilde{g_{ij}}$ | 13.7 | $g_{ij}$ | $k_B$ nK $\mu$m |
| $\tilde{\omega}$ | $4.5 \times 10^3$ | $\omega$ | hertz |
| $\tilde{u_0}^2$ | 33.9 | $u_0^2$ | $k_B$ nK |
| $\tilde{u}(\tilde{x},\tilde{t})$ | $1.57 \times 10^3$ | $u(x,t)$ | $\frac{1}{\sqrt{\text{meter}}}$ |
| $\tilde{v}(\tilde{x},\tilde{t})$ | $1.57 \times 10^3$ | $v(x,t)$ | $\frac{1}{\sqrt{\text{meter}}}$ |

we found numerically that in order to find a bright component in a dark-bright soliton the density of the bright component is required to be less than the density of the dark component. This result was supported by analytical calculations in Sec. II C, where we found that in order to make the dark and bright components oscillate we must meet this criterion. In Sec. III, we calculated different aspects of the interaction between the two components. Of particular interest is the two-component oscillation in the dark-bright soliton, for which we found that the oscillation frequency is nearly independent of the imprinted phase up to a critical value, meaning that the frequency is amplitude independent. We illustrated the oscillation of the density and the phase of the two-component dark-bright soliton. Also, we calculated the binding energy of the dark-bright soliton. We compared the binding energy to the kinetic energy and the mean-field energy of the dark-bright soliton in order to find the critical value of the imprinted phase on the bright component that breaks or unbinds the dark-bright soliton. Future work may extend our study to three-component solitons in different hyperfine states of the same condensate or for different species of atoms. In the multicomponent case, the phase between the different components is coherent, and the norm is not separately conserved.

## ACKNOWLEDGMENTS

We thank U. Al-Khawaja, J. Anderson, and B. Malomed for useful discussions. This material is based in part upon work supported by the National Science Foundation under Grant No. PHY-1306638 and the Air Force Office of Scientific Research under Grant No. FA9550-14-1-0287.

## APPENDIX: FIXED-POINT SINGULARITY

Here we wish to prove that the system of equations (9) does not possess a singularity. In particular, Eq. (9a) with $l \equiv b(t) - d(t)$ becomes

$$\begin{aligned}\frac{d}{dt}\phi_1(t) &= \alpha \operatorname{csch}\left(\frac{l}{w}\right)^4 \left\{2l\left[2+\cosh\left(2\frac{l}{w}\right)\right] - 3w\sinh\left(2\frac{l}{w}\right)\right\} \\ &= 4l\alpha\operatorname{csch}\left(\frac{l}{w}\right)^4 + 2l\alpha\cosh\left(2\frac{l}{w}\right)\operatorname{csch}\left(\frac{l}{w}\right)^4 \\ &\quad - 3w\alpha\operatorname{csch}\left(\frac{l}{w}\right)^4 \sinh\left(2\frac{l}{w}\right).\end{aligned}$$

When we expand the right-hand side of the above equation around the fixed point, the terms $l^{-3}$ and $l^{-1}$ cancel out, and we are left with terms proportional to $l$. That is, the fixed point of the system (i.e., $l = 0$) is valid. Note that we will not be able to address this fact if we work with Eq. (11) instead of Eqs. (9).

[1] T. Dauxois and M. Peyrard, *Physics of Solitons* (Cambridge University Press, Cambridge, 2006).
[2] P. G. Kevrekidis, D. J. Frantzeskakis, R. Carretero-González, N. G. Parker, B. Jackson, A. M. Martin, and C. S. Adams, *Emergent Nonlinear Phenomena in Bose-Einstein Condensates*, Springer Series on Atomic, Optical, and Plasma Physics Vol. 45 (Springer, Berlin, 2008).
[3] P. G. Kevrekidis, D. J. Frantzeskakis, and R. Carretero-González, *The Defocusing Nonlinear Schrodinger Equation: From Dark Solitons to Vortices and Vortex Rings* (Society for Industrial and Applied Mathematics, Philadelphia, 2015).
[4] C. Becker, S. Stellmer, P. Soltan-Panahi, S. Dorscher, M. Baumert, E.-M. Richter, J. Kronjager, K. Bongs, and K. Sengstock, Oscillations and interactions of dark and dark-bright solitons in Bose-Einstein condensates, Nat. Phys. **4**, 496 (2008).
[5] Th. Busch and J. R. Anglin, Dark-Bright Solitons in Inhomogeneous Bose-Einstein Condensates, Phys. Rev. Lett. **87**, 010401 (2001).
[6] V. Achilleos, D. Yan, P. G. Kevrekidis, and D. J. Frantzeskakis, Dark-bright solitons in Bose-Einstein condensates at finite temperatures, New J. Phys. **14**, 055006 (2012).
[7] C. Hamner, J. J. Chang, P. Engels, and M. A. Hoefer, Generation of Dark-Bright Soliton Trains in Superfluid-Superfluid Counterflow, Phys. Rev. Lett. **106**, 065302 (2011).
[8] S. Rajendran, P. Muruganandam, and M. Lakshmanan, Interaction of dark-bright solitons in two-component Bose-Einstein condensates, J. Phys. B **42**, 145307 (2009).
[9] X.-F. Zhang, X.-H. Hu, X.-X. Liu, and W. M. Liu, Vector solitons in two-component Bose-Einstein condensates with tunable interactions and harmonic potential, Phys. Rev. A **79**, 033630 (2009).
[10] M. A. Hoefer, J. J. Chang, C. Hamner, and P. Engels, Dark-dark solitons and modulational instability in miscible two-component Bose-Einstein condensates, Phys. Rev. A **84**, 041605 (2011).
[11] F. Kh. Abdullaev, A. Gammal, A. M. Kamchatnov, and L. Tomio, Dynamics of bright matter wave solitons in a Bose-Einstein condensate, Int. J. Mod. Phys. B **19**, 3415 (2005).
[12] V. M. Pérez-García and J. V. Beitia, Symbiotic solitons in heteronuclear multicomponent Bose-Einstein condensates, Phys. Rev. A **72**, 033620 (2005).
[13] T. Karpiuk, M. Brewczyk, S. Ospelkaus-Schwarzer, K. Bongs, M. Gajda, and K. Rzażewski, Soliton Trains in Bose-Fermi Mixtures, Phys. Rev. Lett. **93**, 100401 (2004).
[14] D. J. Kaup, B. A. Malomed, and R. S. Tasgal, Internal dynamics of a vector soliton in a nonlinear optical fiber, Phys. Rev. E **48**, 3049 (1993).
[15] B. A. Malomed, Polarization dynamics and interactions of solitons in a birefringent optical fiber, Phys. Rev. A **43**, 410 (1991).
[16] J. Scheuer and M. Orenstein, Forces and equilibrium states between interacting vector solitons, J. Opt. Soc. Am. B **18**, 954 (2001).
[17] Y. V. Kartashov, V. A. Vysloukh, L. Torner, and B. A. Malomed, Self-trapping and splitting of bright vector solitons under inhomogeneous defocusing nonlinearities, Opt. Lett. **36**, 4587 (2011).

[18] V. V. Afanasyev, Y. S. Kivshar, V. V. Konotop, and V. N. Serkin, Dynamics of coupled dark and bright optical solitons, Opt. Lett. **14**, 805 (1989).

[19] D. J. Frantzeskakis, Dark solitons in atomic Bose-Einstein condensates: From theory to experiments, J. Phys. A **43**, 213001 (2010).

[20] R. Carretero-González, D. J. Frantzeskakis, and P. G. Kevrekidis, Nonlinear waves in Bose-Einstein condensates: Physical relevance and mathematical techniques, Nonlinearity **21**, R139 (2008).

[21] X. Liu, H. Pu, B. Xiong, W. M. Liu, and J. Gong, Formation and transformation of vector solitons in two-species Bose-Einstein condensates with a tunable interaction, Phys. Rev. A **79**, 013423 (2009).

[22] L. Qiu-Yan, L. Zai-Dong, Y. Shu-Fang, L. Lu, and F. Guang-Sheng, Formation of combined solitons in two-component Bose Einstein condensates, Chin. Phys. B **19**, 080501 (2010).

[23] Z. Xiao-Fei, Z. Pei, H. Wan-Quan, and L. Xun-Xu, Stability properties of vector solitons in two-component Bose-Einstein condensates with tunable interactions, Chin. Phys. B **20**, 020307 (2011).

[24] S. K. Adhikari, Phys. Lett. A **346**, 179 (2005).

[25] C.-F. Liu, M. Lu, and W.-Q. Liu, Dynamics of vector dark soliton induced by the Rabi coupling in one-dimensional trapped Bose-Einstein condensates, Phys. Lett. A **376**, 188 (2012).

[26] D. Yan, J. J. Chang, C. Hamner, M. Hoefer, P. G. Kevrekidis, P. Engels, V. Achilleos, D. J. Frantzeskakis, and J. Cuevas, Beating dark-dark solitons in Bose-Einstein condensates, J. Phys. B **45**, 115301 (2012).

[27] S. Middelkamp, J. J. Chang, C. Hamner, R. Carretero-González, P. G. Kevrekidis, V. Achilleos, D. J. Frantzeskakis, P. Schmelcher, and P. Engels, Dynamics of dark-bright solitons in cigar-shaped Bose-Einstein condensates, Phys. Lett. A **375**, 642 (2011).

[28] H. Li, D. N. Wang, and Y. Cheng, Dynamics of dark-bright vector solitons in a two-component Bose-Einstein condensate, Chaos Solitons Fractals **39**, 1988 (2009).

[29] B. A. Malomed, Internal vibrations of a vector soliton in the coupled nonlinear Schrodinger equations, Phys. Rev. E **58**, 2564 (1998).

[30] J. Goldstone, Field theories with superconductor solutions, Nuovo Cimento **19**, 154 (1961).

[31] L. D. Carr and M. A. Leung, Dynamics of the Bose-Einstein condensate: Quasi-one-dimension and beyond, J. Phys. B **33**, 3983 (2000).

[32] Y. S. Kivshar and W. Królikowski, Lagrangian approach for dark solitons, Opt. Commun. **114**, 353 (1995).

[33] Y. S. Kivshar and B. Luther-Davies, Dark optical solitons: Physics and applications, Phys. Rep. **298**, 81 (1998).

[34] T. Ueda and W. L. Kath, Dynamics of coupled solitons in nonlinear optical fibers, Phys. Rev. A **42**, 563 (1990).

[35] We note that the simplification of Eq. (11) produces the same eigenfrequencies, as we verified that using an independent calculation.

[36] A. Roy and D. Angom, Fluctuation- and interaction-induced instability of dark solitons in single and binary condensates, Phys. Rev. A **90**, 023612 (2014).